Progress In Electromagnetics Research M, Vol. 106, 25–34, 2021

Optimal Magnetic Wake Detection in Finite Depth Water

Mohammad-Amir Fallah[1, *] and Mehdi Monemi[2]

Abstract—Seawater is generally considered as an electrical conductor with rather weak electrical conductivity. As a moving electrical conductor in an electromagnetic field, seawater motions induce weak electromagnetic field in surrounding environment. The movement of vessels in seawater leads to the variations of electromagnetic field pattern, called as magnetic wake. In order to detect a moving object through the induced magnetic wake, a magnetometer can be placed under the seawater surface. In this paper, we present a mathematical model through which we can study the magnetic wake in water of finite depth and, explore its behavior with respect to environmental parameters and geometric characteristics of the moving object. More specifically, we show through mathematical expressions and numerical results that there always exists an optimal depth under the sea surface wherein if a magnetometer is placed, maximum amplitude of magnetic wake can be captured. Several key properties are verified for the optimal magnetic wake detection through numerical results. Firstly, the optimal depth is increased by increasing the speed of the moving vessel. Secondly, the optimal depth is not influenced considerably by the variation of sea depth, and thirdly, in the case where the Froude number of the vessel is lower than 0.5, the optimal depth is below 15 m.

1. INTRODUCTION

The detection of distant vessels in seas and oceans has always been an issue of interest. A moving vessel causes changes in different parameters in the surrounding environment through which one can detect its existence without seeing the vessel. Basically, one can detect the vessel from far distances through considering the most affected environmental parameters. The basic and most traditional method for the vessel detection is to listen to the changes of environmental sounds; however, this scheme was gradually suppressed due to technological advances in designing vessels with more acoustic silence. On the other hand, the development of high precision electronic devices and sensors has directed remote sensing schemes at seawater to employing marine electromagnetic techniques. Efficient implementation of remote sensing schemes for vessels through electromagnetic signal measurement requires highly accurate magnetic sensors. Moreover, due to the large dimensions of hydro-physical changes, hydrodynamic harmonics in the seawater are considered as low frequency ones. Therefore, accurate magnetic sensor with the accuracy of less than 1 pico-Tesla (pT) and low frequency measuring capability is essential to the implementation of efficient remote sensing techniques [1–5]. Once a high-quality signal is measured through a magnetic sensor, the implementation of signal processing techniques is required in order to accurately distinguish the signal from remote vessel out of environmental noise and disturbances [6, 7].

The processing data measured through high precision magnetic sensors can lead to the detection of vessel or the estimation of vessel parameters when sufficient knowledge of the hydrodynamic perturbation of the vessel motion is available. The movement of a vessel results in fluid turbulence behind the vessel called as hydrodynamic wake [8]. Studies show that this wake has a V-shape hydrodynamic

Received 15 September 2021, Accepted 24 November 2021, Scheduled 26 November 2021

* Corresponding author: Mohammad-Amir Fallah (mfallah@shirazu.ac.ir).

[1] Department of Engineering, Payame Noor University (PNU), Tehran, Iran. [2] Department of Electrical Engineering, Salman Farsi University of Kazerun, Kazerun, Iran.

pattern that distinguishes it from marine ambient noise [9]. The characteristics of a vessel hydrodynamic wake are related to environmental parameters and physics of the vessel [10]. The most important feature of a vessel hydrodynamic wake from the point of remote sensing is its ability to propagate the pattern up to tens of kilometers and its durability up to hours [11]. On the other hand, seawater is a poor conductor of electricity. The motion of seawater as a conductor moving in a geomagnetic field induces a weak magnetic anomaly whose properties are similar to hydrodynamic wake [12, 13]. The movement of a ship in conducting seawater and the creation of a hydrodynamic wake within the Earth's magnetic field cause a magnetic wake, which has all the characteristics of hydrodynamic wake [14, 15], so it can be used as a good tool to detect a moving vessel and estimate its physical parameters such as speed and moving direction [16, 17].

Till now, there have been many research studies on the constitution of the magnetic wake in deep water, and its relation to environmental parameters as well as the physical specifications of the vessel [18, 19]. The far field study of magnetic anomaly in shallow water has been directed by [20–22]. While theoretical calculations have been conducted for a Havelock point source [23] and slender body [24] for both near and far fields, none have considered the effect of the physical shape of the vessel. Due to the very small amplitude of the magnetic wake at long distances from the vessel, various methods have been proposed in order to overcome this problem. In [17], the implementation of airborne magnetic transducer measuring the first order gradients of the magnetic wake has been considered. The limited flight time and the high speed movement of the airborne sensor, which leads to an increase in the sample rate and bandwidth of the magnetic sensor, are among the disadvantages of this method. As another approach, the implementation of a linear array of magnetic sensors has been presented in [22]. In this method, the sensor array is installed on the water surface, and a signal processing scheme is proposed in order to increase the detection range.

In this paper, we focus on the study of far field wake in the water of finite depth. At first, we express the magnetic wake pattern formulations in finite depth water initiated from a moving vessel and analyze its variation as a function of the distance from the vessel. We include the physical shape parameters of the vessel in the presented mathematical expressions, and thus our derived results are not limited to slender body theory. Similar to [17] and [22], we analyze the frequency spectrum of the magnetic wake and show that the magnetic anomaly initiated from the moving vessel can be distinguished from the background geomagnetic noise by exploring the frequency spectrum of the measured signal. Based on analyzing the magnetic wake behavior, it is shown that the amplitude of magnetic anomaly decreases exponentially as the distance of the moving vessel increases, and thus, it is of great importance to install the magnetometer sensor in the right place in order to receive the maximum magnetic anomaly. In this regard, we will further show that there exists an optimal depth under the sea surface at which maximum magnetic anomaly can be captured. We will show that the optimal depth does not depend on the sea depth, and for the case where the magnetometer is placed at this optimal point, it can distinguish farthest possible vessels by detecting the maximum amplitude of the magnetic wake. The higher the speed of the vessel is, the deeper the optimal point would be, and furthermore we will verify that for the case when vessel Froude number is lower than 0.5, the optimal depth for sensor installations is less than 15 m. The rest of the paper is organized as follows. In Section 2, the hydrodynamic preliminaries of the vessel wake are discussed, and the relation of the hydrodynamic wake to the shape and speed of the vessel is mathematically formulated. Section 3 studies the corresponding geomagnetic anomaly resulting from the hydrodynamic wake coupled with the electromagnetic environmental parameters according to the Maxwell equations. In Section 4 shows that the magnetic wake can be distinguished from the ambient noise through frequency domain analysis. In Section 5, it is proved that there always exists a unique optimal depth wherein if the magnetic sensor is positioned, maximum anomaly can be captured. Theoretical findings are finally verified through numerical results in Section 6.

2. HYDRODYNAMIC PRELIMINARIES

The movement of a floating body in a fluid instigates two regimes of near field and far field hydrodynamic anomaly. Here, we are mainly involved with the far field regime (called as Kelvin waves [8, 9]) because we are interested in detecting far vessels. The velocity potential function of the fluid (i.e., the sea) resulting from the movement of a floating body at speed V corresponding to a wave front of angle θ

with respect to the x axis is given as follows [8]:

$$\phi(x,y,z,t,\theta) = \frac{A_\theta g}{\omega_0}\frac{\cosh k_0(z+d)}{\cosh k_0 d}\, e^{-i(\omega_0 t + k_0 x\cos\theta + k_0 y\sin\theta)}, \tag{1}$$

where g is the gravity force, d the sea depth, and k_0 the wavenumber which is obtained from $k_0 \tanh k_0 d = \omega_0^2/g$, in which $\omega_0 = k_0 V\cos\theta$ is the Doppler relation. A_θ is obtained from the following equation [10]:

$$A_\theta = \frac{2\omega_0 g}{\cos^3\theta \pi V^3}\frac{e^{k_0 d} - e^{-k_0 d}}{e^{2k_0 d} - e^{-2k_0 d} - 4k_0 d}\,\kappa_\theta, \tag{2}$$

where κ_θ is called as the Kochin function defined as follows [10]:

$$\kappa_\theta = \iint\limits_s I_\kappa\left(x', y', z'\right) e^{-ik_0(x'\cos\theta + y'\sin\theta)} \times \cosh k_0\left(z' + d\right) dx' dy', \tag{3}$$

in which s is the wetted cross-sectional area of the vessel, and I_κ represents the dependence of the Kochin function to the physical parameters of the floating body (such as the shape of the vessel). Finally, the fluid velocity vector resulting from the movement of the vessel is obtained as:

$$\mathbf{U} = \boldsymbol{\nabla}\phi. \tag{4}$$

3. GEOMAGNETIC PRELIMINARIES

Consider a fluid with a flat surface, and also consider the Cartesian coordinate system, wherein the z-axis is perpendicular to the fluid surface, and $z > 0$ corresponds to the space above the fluid. The positive direction of x axis is aligned with the movement of the vessel, and the direction of y axis is found according to the right-hand law. The unit vector in Cartesian coordinate is denoted by $\mathbf{r} = (\mathbf{i}, \mathbf{j}, \mathbf{k})$. The geomagnetic field of the earth (denoted by $\mathbf{B}_E$) is considered to be constant everywhere, and a vessel is located at the origin at time $t = 0$ and moves at uniform speed $\mathbf{V}$ at $-x$ direction. This results in the formation of hydrodynamic wake with velocity $\mathbf{U}$. Let $\boldsymbol{\sigma} = (\sigma_a, \sigma_w, \sigma_s)$, $\boldsymbol{\varepsilon} = (\varepsilon_a, \varepsilon_w, \varepsilon_s)$ and $\boldsymbol{\mu} = (\mu_a, \mu_w, \mu_s)$ be the electrical conductivity coefficient, dielectric coefficient, and magnetic permeability coefficient for $z > 0$ (i.e., air), $-d < z \leq 0$ (i.e., water), and $z \leq -d$ (i.e., under the seabed), respectively. The geomagnetic equations relating to the three aforementioned layers are simply the Maxwell equations for electric and magnetic fields $\mathbf{E}$ and $\mathbf{B}$, as well as the Ohm law for electrical conductors. Let ρ_e denote the electrical flux density. The Maxwell equations in the three aforementioned regions are shown as Eq. (5),

$$\nabla\times\mathbf{B} = \begin{cases} \mu_a\varepsilon_a\dfrac{\partial\mathbf{E}}{\partial t}, & z > 0 \quad \text{a) air} \\ \mu_w\varepsilon_w\dfrac{\partial\mathbf{E}}{\partial t} + \mu_w\sigma_w\left(\mathbf{E} + \mathbf{U}\times\mathbf{B}_T\right) + \mu_w\rho_e\mathbf{U} & \\ +\mu_w\left(\varepsilon_w - \varepsilon_0\right)\nabla\times\left(\mathbf{E} + \mathbf{U}\times\mathbf{B}_T\right)\times\mathbf{U}, & -d < z < 0 \quad \text{b) fluid} \\ \mu_s\varepsilon_s\dfrac{\partial\mathbf{E}}{\partial t} + \mu_s\sigma_s\mathbf{E}, & z < -d \quad \text{c) soil} \end{cases} \tag{5}$$

where $\mathbf{B}_T = \mathbf{B} + \mathbf{B}_E$, in which $\mathbf{B}_E$ is the geomagnetic field, and $\mathbf{B}$ represents the magnetic wake. In practice, the magnitude of the induced magnetic wave is much smaller than that of geomagnetic field, and thus we can approximate $\mathbf{B}_T \approx \mathbf{B}_E$ with high precision. In order to obtain the solution to Eq. (5), one should note the nature of the potential function of ϕ in Eq. (1) and thus consider the harmonic behavior of $\mathbf{U}$ as well as that of $\mathbf{B}$ and $\mathbf{E}$. The electric and magnetic harmonic fields are respectively written as:

$$\begin{aligned} \mathbf{H} &= \mathbf{h}(\theta, z)\, e^{-i(\omega_0 t + k_0 x\cos\theta + k_0 y\sin\theta)} \\ \mathbf{E} &= \mathbf{e}(\theta z) e^{-i(\omega_0 t + k_0 x\cos\theta + k_0 y\sin\theta)} \end{aligned} \tag{6}$$

The single-component harmonic solution for the magnetic wake is obtained as follows:

$$\begin{aligned} \mathbf{h}(\theta, z) \;=\; & \mathbf{h}^a(\theta)\, e^{-\beta_a z}\tau(z) + \mathbf{h}^s(\theta)\, e^{\beta_s(z+d)}\tau(-z-d) \\ & + \left[\mathbf{h}_w^+(\theta)\, e^{\beta_w z} + \mathbf{h}_w^-(\theta)\, e^{-\beta_w z} + \mathbf{a}_w^+(\theta)\, e^{k_o z} + \mathbf{a}_w^-(\theta)\, e^{-k_o z}\right]\tau(z+d)\,\tau(-z) \end{aligned} \tag{7}$$

in which $\tau(z)$ is the unit step function, $\beta_a^2 = k_0^2 - \varepsilon_a\mu_a\omega_0^2$, $\beta_w^2 = k_0^2 - \varepsilon_w\mu_w\omega_0^2 - i\sigma_w\mu_w\omega_0$, $\beta_s^2 = k_0^2 - \varepsilon_s\mu_s\omega_0^2 - i\sigma_s\mu_s\omega_0$, and

$$\mathbf{a}_w^+(\theta) = \frac{k_o\sigma_w}{\left(k_0^2 - \sigma_w^2\right)} \frac{e^{k_o d}}{e^{k_o d} + e^{-k_o d}} \left[i\left(\mathbf{B}_E \cdot \mathbf{r}\right) - \left(\mathbf{B}_E \cdot \mathbf{k}\right)\right] \left[i\cos\theta, i\sin\theta, 1\right] \tag{8}$$

$$\mathbf{a}_w^-(\theta) = \frac{k_o\sigma_w}{\left(k_0^2 - \sigma_w^2\right)} \frac{e^{k_o d}}{e^{k_o d} + e^{-k_o d}} \left[i\left(\mathbf{B}_E \cdot \mathbf{r}\right) + \left(\mathbf{B}_E \cdot \mathbf{k}\right)\right] \left[i\cos\theta, i\sin\theta, -1\right] \tag{9}$$

All unknown coefficients in Eq. (7) are computed by applying continuous boundary conditions in the boundaries of the three mediums. The terms $\mathbf{h}^a(\theta)e^{-\beta_a z}$ and $\mathbf{h}^s(\theta)e^{\beta_s(z+d)}$ in Eq. (7) respectively denote the wave motion in the air and under the seabed, respectively; however for water, this corresponds to the movement of two waves in opposite directions. The magnetic wake can eventually be computed by applying superposition for all harmonic components expressed as follows:

$$\mathbf{H}(x, y, z, t) = \Re \int_{\pi/2}^{\pi/2} \mathbf{h}(\theta, z) A_\theta e^{-i(\omega_0 t + k_0 x\cos\theta + k_0 y\sin\theta)} d\theta \tag{10}$$

One can verify that all results are applicable to the deep water as well by considering $d \to \infty$ [14].

4. INVESTIGATION OF MAGNETIC WAKE PATTERN THROUGH SPECTRUM ANALYSIS

In what follows we investigate the magnetic wake characteristics in frequency domain through which we may distinguish the magnetic wake and discriminate it from the background noise. The magnetic wake measured by a magnetometer at time t and point (x_d, y_d, z_d) is denoted by $\mathbf{H}(x_d, y_d, z_d, t)$ which is expressed through Eq. (10). The corresponding frequency domain representation is expressed as follows:

$$\hat{H}(f) = \left[\int_0^t \mathbf{H}(x_d, y_d, z_d, t)\, e^{-i(2\pi f)t} dt\right] = \frac{\mathbf{h}(\theta_0, z_d) A(\theta_0)\, e^{-\beta_a z_d} e^{-i\emptyset_0(\theta_0)}}{|\phi'(\theta_0)|} \tag{11}$$

in which:

$$\phi_0(\theta) = k_0(\theta)\left(x_0\cos\theta + y_0\cos\theta\right) \tag{12}$$

$$\phi(\theta) = \frac{-k_0(\theta)V\sin\theta}{2\pi\cos^2\theta} \tag{13}$$

and θ_0 is the root of equation $|\phi(\theta)| = f$. It is seen from Eq. (11) that there exists some frequency corresponding to $|\phi'(\theta_0)| \to 0$ wherein the magnetic wake has a large amplitude. This property can be used to distinguish the magnetic wake out of the ambient noise. Hence, having the time-domain behavior of the magnetic wake, we may transfer it to frequency domain and investigate the existence of a peak at some specified frequency, through which one can distinguish the existence of a floating or submerged vessel. It is clear that higher time-domain magnetic anomaly captured through the magnetic sensor results in higher peak amplitude of the corresponding frequency-domain signal. Thus, it is vital to place the sensor at the optimal point wherein maximum anomaly can be captured.

5. OPTIMAL DEPTH DETERMINATION

Based on what stated so far, we aim at finding the optimal location point of the magnetometer at which the measured magnetic wake is maximum, resulting in the maximum probability of remote vessel detection. As mentioned before, the magnetic anomaly can be observed in any of the three mediums of air, water, and under the seabed. The question is where to place the magnetometer in order to measure the maximum amplitude of the magnetic wake. From Eq. (10), it is seen that the variation of the amplitude of magnetic wake in horizontal directions of x and y takes place in the form of

harmonics whose amplitudes are decreased as the relative distance of the vessel and magnetometer increases. It is clear that due to the fixed position of the magnetometer, the relative horizontal distance (at x and y directions) between the magnetometer and vessel is only dependent upon the position of the vessel, and thus, the only accessible and effective location parameter is the distance between the magnetometer and surface of water (i.e., z). On the other hand, it is seen in Eq. (10) that $\mathbf{h}(\theta, z)$ is the only component which depends on z. From Eq. (7), the amplitude of magnetic wake in the air is seen to decrease exponentially according to $\mathbf{h}^a(\theta)e^{-\beta_a z}$ as the altitude increases, and it decreases under the seabed according to $\mathbf{h}^s(\theta)e^{\beta_s(z+d)}$ as the depth increases. However, in the water between the air and the seabed, the variation of the amplitude of magnetic wake is not a monotonic function of z. In this region, the magnetic wake is composed of two waves travelling in opposite directions with propagation constants β_w and $-\beta_w$, and thus we expect that there exists some local optimal depth below and above which the magnetic wake is reduced. Thus, we may calculate the optimal depth for $-d \leq z < 0$ denoted by $\mathbf{z}^* = (z_x^*, z_y^*, z_z^*)$ as the solution to the following problem:

$$\frac{\boldsymbol{\partial}\mathbf{H}\,(x, y, z, t)}{\boldsymbol{\partial}\mathbf{z}} = 0 \tag{14}$$

Note that Eq. (14) is a vector equation, and thus, for each of the elements of (H_x, H_y, H_z) we may find the corresponding optimal $\mathbf{z}^*$ separately. Therefore, depending on which one of the magnetic harmonic elements is considered for the detection, the magnetometer should be placed on the corresponding solution of the optimal depth problem expressed in Eq. (14). In summary from what has been discussed so far, the following procedure derives the unique optimal depth h^{opt} wherein the maximum magnetic wake can be captured:

1- Consider the following parameters: $\kappa_\theta, V, d, \boldsymbol{\varepsilon}, \boldsymbol{\sigma}, \boldsymbol{\mu}$.
2- Calculate A_θ from Eqs. (2) and (3).
3- Obtain $\phi(x, y, z, t, \theta)$ from Eq. (1).
4- Obtain $\mathbf{U}$ from Eq. (4).
5- Substitute single-component harmonic solution from Eq. (6) into (5), and then solve Eq. (5) in order to obtain $\mathbf{h}(\theta, z)$.
6- Calculate $\mathbf{H}(x, y, z, t)$ by applying superposition on $\mathbf{h}(\theta, z)$ according to Eq. (10).
7- From Eq. (7), the existence of a unique optimal depth h^{opt} is proven where h^{opt} can be obtained by calculating the derivative of $\mathbf{H}(x, y, z, t)$ according to Eq. (14).

6. NUMERICAL RESULTS

In this section, we provide numerical results for different scenarios in order to validate the stated expressions relating to the optimal position of the magnetometer corresponding to the highest detection capability for the moving vessel. We consider a Wigley shape vessel of length 110 m, width 15 m, and draft 5 m moving at speed 10 m/s in the sea water of depth $d = 70$ m. The electric and magnetic parameters are considered as $(\varepsilon_a, \varepsilon_w, \varepsilon_s) = (\varepsilon_0, 81\varepsilon_0, 11\varepsilon_0)$, $(\sigma_a, \sigma_w, \sigma_s) = (0, 5, 0.27)$, and $(\mu_a, \mu_w, \mu_s) = (\mu_0, \mu_0, \mu_0)$ [25–28]. The amplitude of the geomagnetic field is $|\mathbf{B}_E| = 50000$ nT. The vertical component of the magnetic wake is obtained from $B_z = \mu_0 H_z$, wherein H_z is obtained from Eq. (10).

Figure 1 shows the pattern of the vertical component of the geomagnetic anomaly (B_z) in a noiseless area of $800 \times 1000\,\mathrm{m}^2$. Assuming that the magnetometer is located at point $(300, 0, 0)$, the magnetic wake resulting from the movement of the vessel at the location of the sensor is depicted in Fig. 2. It is seen how the amplitude of B_z decreases as the relative distance from the vessel increases. Similarly, for the case where an additive white Gaussian noise (AWGN) is also considered, the amplitude of B_z per time is illustrated in Fig. 3, wherein we have considered SNR = 0 dB. As seen in the figure, it is almost impossible to distinguish the existence of magnetic wake created by the moving vessel from the time-domain figure. Based on what stated, now we study the frequency-domain spectrum of the magnetic wake corresponding to Fig. 3 as illustrated in Fig. 4. It is clearly seen that although the existence of magnetic wake is not clear in time domain figure, the frequency domain spectrum clearly reveals the existence of the remote vessel.

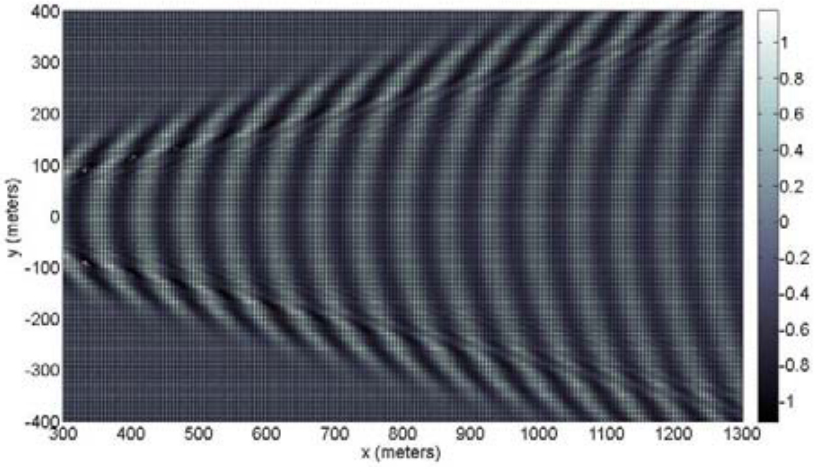

Figure 1. The amplitude (in nT) of vertical component of the magnetic wake B_z at $z = 0\,\mathrm{m}$ and sea depth $d = 70\,\mathrm{m}$.

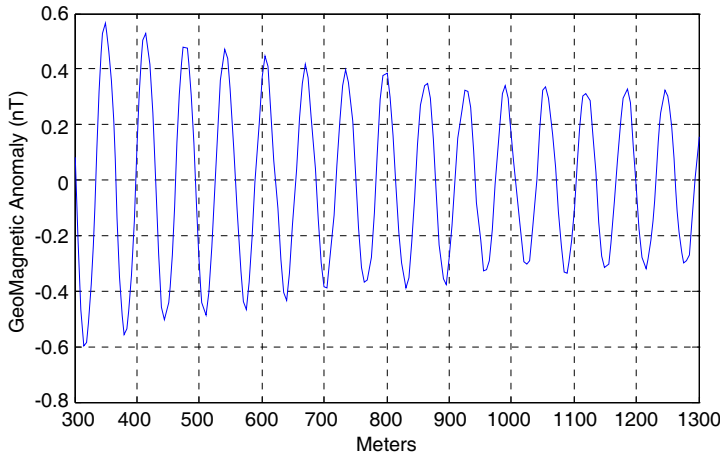

Figure 2. Magnetic wake B_z per distance from the vessel.

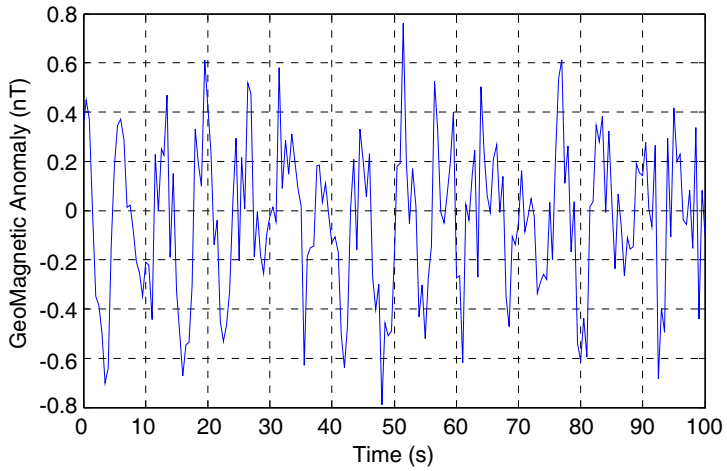

Figure 3. Time-domain magnetic wake B_z in the presence of AWGN SNR $= 0\,\mathrm{dB}$.

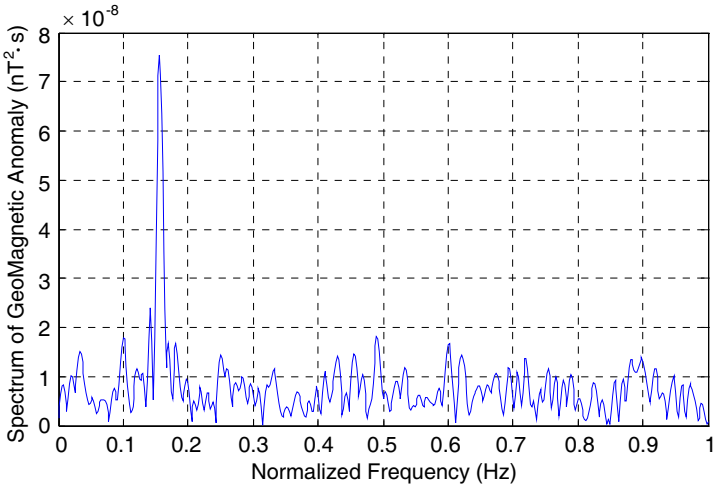

Figure 4. The frequency spectrum of magnetic wake B_z in presence of AWGN SNR = 0 dB.

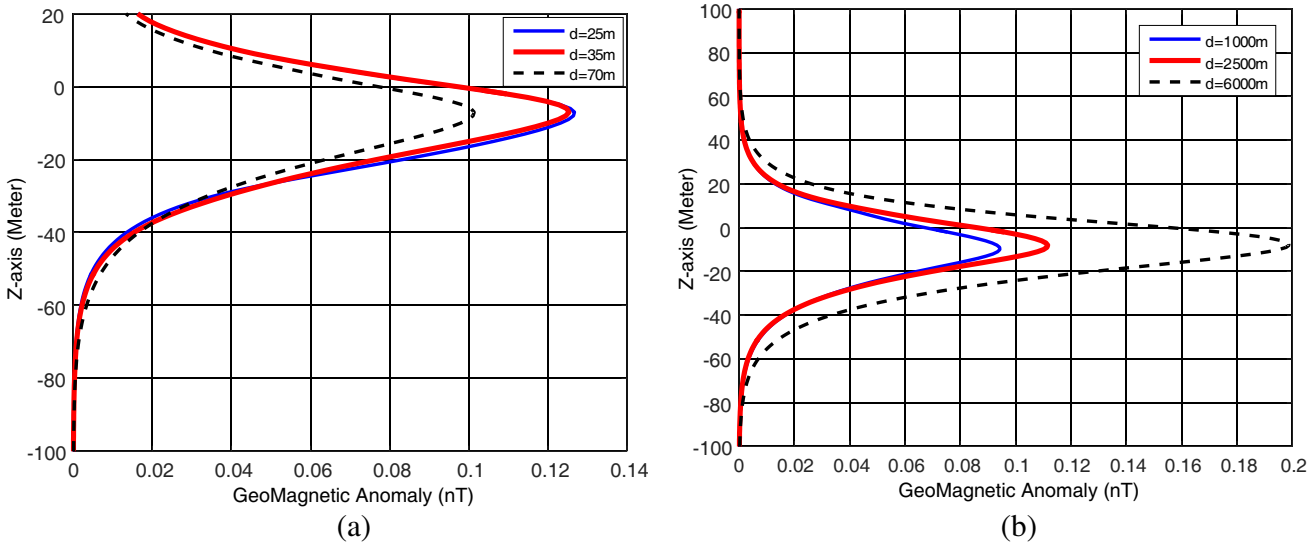

Figure 5. The amplitude of the vertical component of magnetic wake (B_z) at the distance of 5 km from a vessel travelling at speed 10 m/s. (a) Shallow water of depth lower than 100 m. (b) Deep water of depth higher than 1000 m.

As seen in Fig. 2, the increase in the distance between the vessel and magnetometer considerably decreases the measured magnetic wake amplitude; in fact, at rather large distances, the maximum measured amplitude would not be greater than tens of Pico Tesla. Therefore, considering such small measurable amplitudes, it is of great importance to capture the maximum possible amplitude of the magnetic wake to be able to detect remote vessels. In order to evaluate the optimal depth for locating the magnetometer, we consider a magnetometer whose horizontal distance from the vessel is 5 km. The vessel is moving at the speed of 10 m/s in a seawater whose depth is considered to be of values lower than 100 m as shallow water and higher than 1000 m as deep water investigated according to Fig. 5(a) and Fig. 5(b), respectively. The vertical component of the magnetic wake (i.e., B_z) for three different water depths ($d = 25$ m, 35 m, and 70 m for the shallow water, and $d = 1000$ m, 3000 m, and 6000 m for the deep water) versus the distance from water surface (z) is depicted in Fig. 5. As discussed before, the maximum vertical magnetic anomaly is seen to exist at some depth inside the sea water, and the magnetic wake decays exponentially above the water surface as well as below the seabed as shown and

discussed in Section 5. Due to the steep slope of the curves, it is of crucial importance to place the magnetometer at every point corresponding to the optimal peak amplitude; otherwise, the measured amplitude of the wake is exponentially decreased. Another important issue which is observed in Fig. 5 is that the optimal location wherein maximum anomaly exists is rather independent of the water depth and besides, due to the steep decay of the curve in the points around the optimal depth, and it is of crucial importance to locate the sensor exactly at the optimal point.

The increase in the vessel speed results in the rise in Froude number, and besides, it is well known that due to the high value of inertia of motion, the Froude number for common vessels is mostly lower than 0.5. The impact of the value of Froude number on the optimal depth is illustrated in Fig. 6. It is seen that for vessels of higher Froude number, the optimal depth increases, and besides, for the case where the Froude number is below 0.5, the optimal depth is lower than 15 m.

Finally, we explore the magnetic anomaly behavior for low and high values of the speed of vessel.

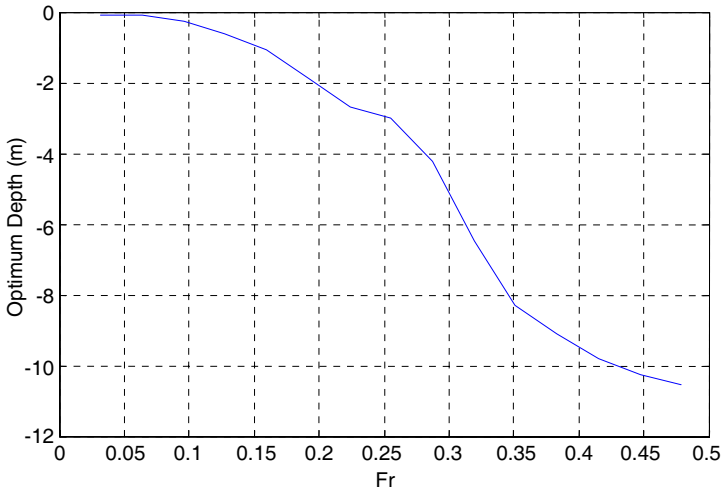

Figure 6. Illustration of the optimal depth (h^{opt}) versus Froude number.

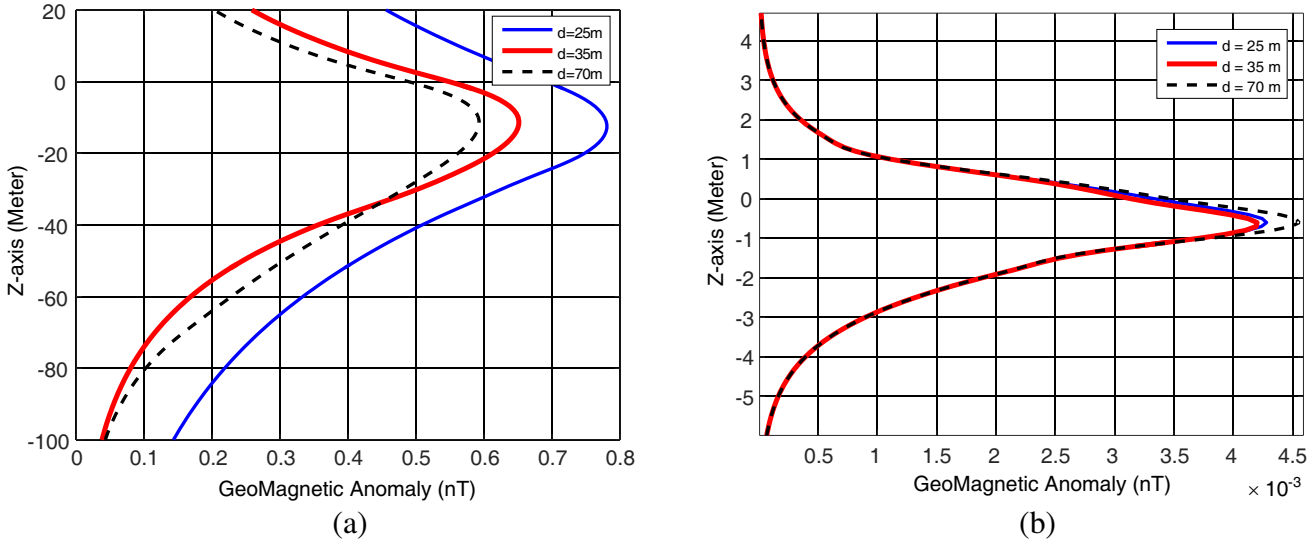

Figure 7. The amplitude of the vertical magnetic wake B_z at the distance of 5 km from a vessel travelling at shallow water of depth 25 , 35 m, and 70 m at (a) the high speed of 15 m/s and (b) the low speed of 1 m/s.

Fig. 7 compares the measured magnetic wake amplitude of B_z versus the vertical position z for the case where the vessel is moving at high speed of 15 m/s and low speed of 1 m/s, corresponding to Fig. 7(a) and Fig. 7(b), respectively. Firstly, by comparing Fig. 7(a) and Fig. 7(b), it is seen that the magnetic anomaly resulting from high-speed vessels is much higher than that of low-speed ones, and thus the former is more easily detected through the measured magnetic wake at farther distances. On the other hand, while the depth of seawater is seen to have little impact on the maximum measured magnetic wake for low-speed vessels, this has rather considerable effect for high-speed vessels. For example, the maximum amplitudes of magnetic wake for $d = 25$ m and $d = 70$ m are 0.77 nT and 0.6 nT for high-speed vessel, and 4.3 pT and 4.6 pT for low-speed one, respectively. This means that for the high-speed vessel, the measured magnetic wake for $d = 70$ m varies about 22% from that of $d = 25$ m; however for the low-speed vessel, the magnetic wake for $d = 70$ is only 7% varying from that of $d = 25$ m. In addition, by comparing Figs. 7(a) and 7(b) and considering Fig. 6, it can be seen that by increasing the vessel speed (Froude number), the optimal depth increases from less than 1 meter in Fig. 7(a) to more than 10 meters in Fig. 7(b).

7. CONCLUSION

In this paper, we have studied the geomagnetic wake resulting from moving vessels as a tool for remote sensing of the existence of vessels traveling in shallow and deep waters. More specifically, we expressed theoretical relations for the calculation of magnetic wake in finite depth water, which depends on the environmental parameters such as electrical and magnetic properties of water and air, as well as the parameters relating to the vessel such as the physical shape and speed of the moving vessel. We showed that the resulting magnetic wake was easily distinguished from the background noise by exploring the corresponding frequency domain behavior. We also revealed that there always exists an optimal depth which if magnetometer is positioned at, the maximum amplitude of magnetic wake is captured, leading to the optimum detection capability of remote vessels. The optimal depth was shown to be independent of the sea depth and be of values lower than 15 m for the case where the Froude number of the vessel is lower than 0.5. Besides, we showed that the optimal depth is an increasing function of the speed and hence the Froude number of vessel.

REFERENCES

1. Mizutani, N. and T. Kobayashi, "Magnetic field vector detection in frequency domain with an optically pumped atomic magnetometer," *IEEE Transactions on Magnetics*, Vol. 48, No. 11, 4096–4099, Nov. 2012.
2. Han, F., S. Harada, and I. Sasada, "Fluxgate and search coil hybrid: A low-noise wide-band magnetometer," *IEEE Transactions on Magnetics*, Vol. 48, No. 11, 3700–3703, Nov. 2012.
3. Wang, Z., M. Deng, K. Chen, M. Wang, Q. Zhang, and D. Zeng, "Development and evaluation of an ultralow-noise sensor system for marine electric field measurements," *Sensors and Actuators A: Physical*, Vol. 213, 70–78, 2014, ISSN0924-4247, https://doi.org/10.1016/j.sna.2014.03.026.
4. Han, F., S. Harada, and I. Sasada, "Fluxgate and search coil hybrid: A low-noise wide-band magnetometer," *IEEE Transactions on Magnetics*, Vol. 48, 3700–3703, 2012.
5. Kawai, J., G. Uehara, T. Kohrin, H. Ogata, and H. Kado, "Three axis SQUID magnetometer for low-frequency geophysical applications," *IEEE Transactions on Magnetics*, Vol. 35, 3974–3976, 1999.
6. Chen, Y. F., P. Wu, W. Zhu, and G. Fang, "An innovative magnetic anomaly detection algorithm based on signal modulation," *IEEE Transactions on Magnetics*, Vol. 56, No. 9, 1–9, Sept. 2020, Art no. 6200609, doi: 10.1109/TMAG.2020.3005896.
7. Zhou, J. , J. Chen, and Z. Shan, "Spatial signature analysis of submarine magnetic anomaly at low altitude," *IEEE Transactions on Magnetics*, Vol. 53, No. 12, 1–7, Dec. 2017, Art no. 6001107, doi: 10.1109/TMAG.2017.2735940.
8. Newman, J. N., *Marine Hydrodynamics*, MIT Press, Cambridge, Massachusetts, 1977.

9. Gu, D. F. and O. M. Phillips, "On narrow V-like ship wakes," *J. Fluid Mech.*, Vol. 275, 301–321, 1988.
10. Kostyukov, A. A., *Theory of Ship Waves and Waves Resistance*, 241–243, Effective Communications Inc., Iowa City, 1968.
11. Gilman, M., A. Soloviev, and H. Graber, "Study of the far wake of a large ship," *J. Atmos. Oceanic Technol.*, Vol. 28, 720–733, 2011.
12. Weaver, J. T., "Magnetic variations associated with ocean waves and swell," *Journal of Geophysical Research*, Vol. 70, 1921–1929, 1965.
13. Sanford, T. B., "Motionally induced electric and magnetic fields in the sea," *Journal of Geophysical Research*, Vol. 76, 3476–3492, 1971.
14. Madurasinghe, D., "Induced electromagnetic fields associated with large ship wakes," *Wave Motion*, Vol. 20, 283–292, 1994.
15. Madurasinghe, D. and E. O. Tuck, "The induced electromagnetic field associated with submerged moving bodies in an unstratified conducting fluid," *IEEE Journal of Ocean Engineering*, Vol. 19, 193–199, 1994.
16. Madurasinghe, D. and G. R. Haack, "The induced electromagnetic field associated with wakes-signal processing aspects," *Proceedings of IGRASS*, Vol. 94, 2335–2357, Pasadena, CA, 1994.
17. Zou, N. and A. Nehorai, "Detection of ship wakes using an airborne magnetic transducer," *IEEE Transactions on Geoscience and Remote Sensing*, Vol. 38, No. 1, 532–539, Jan. 2000, doi: 10.1109/36.823948.
18. Fallah, M. A. and H. Abiri, "Electromagnetic fields induced by the motion of Di-Hull bodies in a conducting fluid," *IEEE Transactions on Magnetics*, Vol. 49, No. 10, 5257–5263, Oct. 2013, doi: 10.1109/TMAG.2013.2260345.
19. Guo, X., D. Zhao, and Z. Cao, "Detection of the magnetic field induced by the wake of a moving submerged body using simple models," *American Journal of Electromagnetics and Applications*, Vol. 4, No. 2, 20–25, 2016, doi: 10.11648/j.ajea.20160402.12.
20. Chaillout, J. J., J. Berthier, and R. Blanpain, "Modelling of electromagnetic wakes of moving submerged bodies in stratified sea water," *IEEE Transactions on Magnetics*, Vol. 32, No. 3, 998–1001, May 1996, doi: 10.1109/20.497408.
21. Yaakobi, O., G. Zilman, and T. Miloh, "Detection of the electromagnetic field induced by the wake of a ship moving in a moderate sea state of finite depth," *J. Engrg. Math.*, Vol. 70, 17–27, 2011.
22. Amir Fallah, M. and H. Abiri, "Multi-sensor approach in vessel magnetic wake imaging," *Wave Motion*, Vol. 51, 60–76, 2014.
23. Xu, Z., C. Du, and M. Xia, "Evaluation of electromagnetic fields induced by wake of an undersea-moving slender body," *IEEE Access*, Vol. 6, 2943–2951, 2018, doi: 10.1109/ACCESS.2017.2786246.
24. Xu, Z. H., C. P. Du, and M. Y. Xia, "Electromagnetic fields due to the wake of a moving slender body in a finite-depth ocean with density stratification," *Sci. Rep.*, Vol. 8, 14647, 2018, https://doi.org/10.1038/s41598-018-32789-1.
25. Robert, P., *Electrical and Magnetic Properties of Materials*, Artech House, 1988.
26. Schon, J. H., "Physical properties of rocks: Fundamentals and principles of petrophysics Calculated from field data at Otis MMR," *Cape Cod*, Massachusetts, 1996.
27. Mavko, G., *The Rock Physics Handbook: Tools for Seismic Analysis in Porous Media*, Cambridge University Press, 1998.
28. Carmichael, R. S., *Practical Handbook of Physical Properties of Rocks and Minerals*, CRC Press, 1989.